Ancilla-free measurement of out-of-time-ordered correlation functions: General measurement protocol and Rydberg atom implementation

Michael Kastner [1,2] Philip Osterholz [3] and Christian Gross [3]

[1] *Institute of Theoretical Physics, University of Stellenbosch, Stellenbosch 7600, South Africa*

[2] *Hanse-Wissenschaftskolleg, Lehmkuhlenbusch 4, 27753 Delmenhorst, Germany*

[3] *Physikalisches Institut, Eberhard Karls Universität Tübingen, 72076 Tübingen, Germany*

(Received 14 March 2024; accepted 13 June 2024; published 8 July 2024)

We introduce a protocol that gives access to out-of-time-ordered correlation functions in many-body quantum systems. Unlike other such protocols, our proposal, which can be applied to arbitrary initial states, neither requires ancilla degrees of freedom to the quantum system of interest, nor has the need for randomized measurements. Nontrivial experimental capabilities required to implement the protocol are single-site measurements, single-site rotations, and backwards time evolution. To exemplify the implementation of the protocol, we put forward a strategy for Hamiltonian sign inversion $H \to -H$ in arrays of Rydberg-dressed atoms. In this way, a complete and practical toolbox is obtained for the measurement of out-of-time-ordered correlations in equilibrium and nonequilibrium situations.

DOI: 10.1103/PhysRevA.110.013303

"Scrambling" refers to the process where, under unitary time evolution of a many-body quantum system, initially local information disperses into many-body entanglement and spreads over increasingly larger regions of the system. In this process, information, while in principle conserved, becomes inaccessible to local measurements, resulting in an effective loss of memory. Quantum information scrambling rose to prominence in the context of the black hole information problem [1], and accompanies the dynamics of thermalization in isolated quantum systems [2].

A strategy to quantify the size of the region across which quantum information is spread under the system's dynamics consists in considering two operators V and W that are initially supported on separated regions of space, implying $[W, V] = 0$. The commutator $C(t) = \langle |[W(t), V]|^2 \rangle$ then quantifies the degree to which the time-evolved operator $W(t) = \exp(iHt)W\exp(-iHt)$ spreads into the support of V, which indicates whether or not the region over which quantum information can be scrambled in time t extends into the support of V. Moreover, the semiclassical limit of C quantifies the sensitivity of the dynamics to small changes in the initial conditions, which suggests to interpret C as a measure of quantum chaoticity [3]. Closely related to C, and often more practical and accessible, is the out-of-time-ordered correlation (OTOC) [4]

$$F(t) = \langle W^\dagger(t)V^\dagger W(t)V \rangle. \tag{1}$$

Such correlation functions have been used in early studies of electron scattering off impurities in models of superconductors [5], are related to the Renyi entropy and the generation of entanglement [6,7], and have been employed to distinguish many-body localized phases from thermalizing ones [7,8].

A setting of particular physical interest is when V and W are local Hermitian operators that correspond to experimentally measurable observables. But even in such a, presumably "simpler," situation, F in Eq. (1) is the expectation value of a, in general, non-Hermitian and nonlocal operator. A direct measurement of such an expectation value is unrealistic in all but the most trivial special cases, and one therefore has to resort to indirect measurement protocols in order to gain access to OTOCs. Such measurement protocols for OTOCs essentially interpret the product of operators on the right-hand side of Eq. (1) as a sequence of operations. Because of the lack of time-ordering that is characteristic for OTOCs, this sequence of operations involves forward-in-time as well as backward-in-time evolving unitaries, which, while challenging in general, are available in certain experimental platforms such as atoms in optical lattices [9] and in all-to-all interacting neutral atom or ion systems [10–12]. While most of the proposed measurement protocols for OTOCs require backward-in-time evolution, other strategies, each with their own merits and challenges, are known as well [13]. Some aspects of OTOCs have already been measured in small systems [14–19].

Here we will focus on measurement protocols for OTOCs that make use of backwards time evolution. Several such protocols have been proposed by now [20,21], some of which have been implemented experimentally [14,22,23]. While none of these protocols is easy to implement, some are less challenging, but at the expense of being applicable only to specific choices of V and/or specific initial states [14,21,22]. The protocol put forward in Ref. [20], on the other side, is applicable to arbitrary V, W and arbitrary initial states. It is, however, significantly more difficult to implement, as it requires, in addition to backwards time evolution, the capability to couple an ancilla qubit to the system of interest and to create entanglement between the two. An experimental realization of this ancilla-based protocol was reported in Ref. [23] for a two-dimensional array of superconducting qubits, which is known for the exquisite level of experimental controllability.

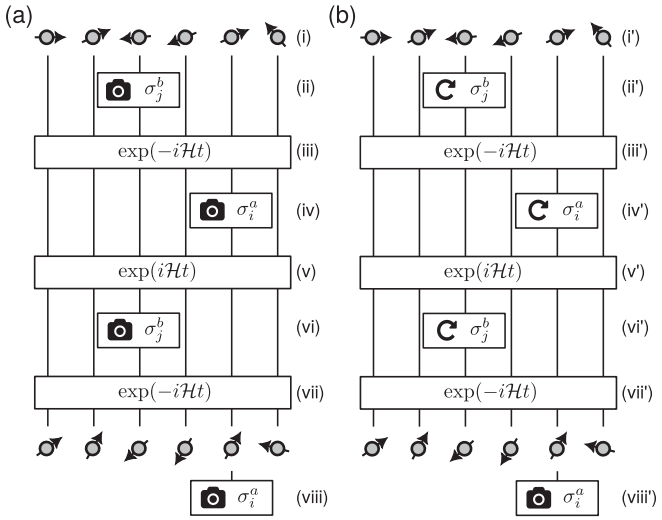

FIG. 1. Sequence of steps for accessing the real part (a) and imaginary part (b) of an OTOC. From top to bottom: (i) initial state, (ii) projective measurement or spin rotation at site j, (iii) forward time evolution under the Hamiltonian H, (iv) projective measurement or spin rotation at site i, (v) backward time evolution under H, (vi) projective measurement or spin rotation at site j, (vii) forward time evolution under H, (viii) projective measurement at site i.

In many other experimental platforms, however, the simultaneous requirements of backwards time evolution and ancilla coupling poses an obstacle. This motivates the search for alternative measurement protocols, ideally of broad applicability and with more moderate experimental requirements.

The first main result of this article is a measurement protocol for OTOCs, applicable to arbitrary initial states, that requires neither ancilla quantum degrees of freedom to be coupled to the system, nor interferometric techniques, nor averaging over randomized initial states. In addition to backwards time evolution, the main experimental requirement to execute the protocol are single-site measurements and single-site rotations in a system of qubits or spin-1/2 degrees of freedom; see Fig. 1 for an illustration. Single-site resolution and addressability are key capabilities of quantum computing platforms and are readily available in a variety of experimental settings.

As the second main result of this article we propose a technique, based on microwave-assisted Rydberg dressing [24], that facilitates Hamiltonian sign inversion, and hence backwards time evolution, in array of ultracold Rydberg-dressed atoms. Combining this technique with local in-sequence readout and local rotation techniques, our measurement protocol becomes a full-fledged tool for the measurement of OTOCs in a relevant experimental platform, while avoiding the challenge of having to couple ancillas to individual sites. Since the protocol is not restricted to specific initial states, OTOCs can be measured and analyzed in arbitrary equilibrium and nonequilibrium situations. The sign-inversion technique is interesting also in the context of other applications, for example, for quantum simulation at finite energies [25] or quantum metrology [26].

I. OTOC MEASUREMENT PROTOCOLS

We consider an arbitrary network of N qubits, which includes regular lattices as special cases. Time evolution is assumed to be unitary, generated by a time-independent Hamiltonian H, but is arbitrary otherwise, allowing for multisite interactions (beyond pair interactions) as well as interactions of arbitrarily long range.

Our main technical requirement is that the operators V and W in Eq. (1) have only two distinct (albeit possibly degenerate) eigenvalues. In the context of qubit systems, this is a very natural and not particularly restrictive setting. For notational simplicity we will in the following choose single-site Pauli spin operators as observables, $W = \sigma_i^a$ and $V = \sigma_j^b$, where i and j denote sites on the network and $a, b \in \{x, y, z\}$ label spin components. The object of study is the OTOC

$$C(t) := \mathrm{Tr}\big[\rho\sigma_i^a(t)\sigma_j^b\sigma_i^a(t)\sigma_j^b\big], \tag{2}$$

where ρ is the initial density operator. Note that, even though each factor of the operator product on the right-hand side of Eq. (2) is Hermitian, the product of operators in general is not, and hence C can be complex.

A. Measurement protocol for the real part

We show that the real part of C can be obtained by interpreting the operator product inside the trace of Eq. (2) as *measurements* of the occurring spin operators, interspersed with time evolutions [27]. This is by no means a trivial statement, as Eq. (2) describes unitary evolution, and measurements are known to disturb unitary evolution due to wave-function collapse. However, when probing bivariate observables, these disturbing effects, which do occur, cancel out exactly when using the following measurement protocol, illustrated in Fig. 1:

(i) Prepare the initial state $|\psi\rangle$.

(ii) Projectively measure the observable σ_j^b and record the outcome ($+$ or $-$).

(iii) Time-evolve unitarily until time t.

(iv) Projectively measure the observable σ_i^a and record the outcome.

(v) Evolve *backwards* in time for a time t.

(vi) Projectively measure the observable σ_j^b and record the outcome.

(vii) Time-evolve unitarily until time t.

(viii) Projectively measure the observable σ_i^a and record the outcome.

(ix) Repeat (i)–(viii) many times and record the relative frequencies of the combinations of measurement outcomes $(++++)$, $(+++-)$, $(++-+)$, etc., occurring in each of the measurement sequences.

(x) Use these relative frequencies to estimate the corresponding probabilities P_{++++}, P_{+++-}, P_{++-+}, etc., and calculate the correlation function

$$\mathscr{C}(t) := \sum_{o_1,o_2,o_3,o_4\in\{-1,+1\}} o_1o_2o_3o_4P_{o_1o_2o_3o_4}. \tag{3}$$

We show in Appendix A that

$$2\mathscr{C}(t) - 1 = \mathrm{Re}C(t), \tag{4}$$

i.e., the real part of the desired OTOC (2) is obtained by applying the above protocol that "naively" disregards the effect of measurement backaction. The key experimental capabilities to execute the protocol are unitary backwards time evolution and projective measurements of single qubits.

B. Unitarily evolved vs projectively measured OTOCs

Equation (4) is an exact relation between the OTOC C and the correlation function $\mathscr{C}$, where the latter is determined by the probabilities $P_{\pm\pm\pm\pm}$. In an experimental realization of the measurement protocol, these probabilities must be estimated through finite sample averages. The sampling introduces statistical errors, which, by error propagation, cause errors in C. We illustrate the magnitude of these errors, and hence the performance of the proposed measurement protocol when constrained by limited resources, for spin chains with nearest-neighbor XZ couplings,

$$H = -\sum_{k=1}^{N-1} \left(\sigma_k^x \sigma_{k+1}^x + \sigma_k^z \sigma_{k+1}^z\right). \tag{5}$$

For this Hamiltonian and using the initial state $\rho = (|\uparrow \cdots \uparrow\rangle \langle\uparrow \cdots \uparrow|)^{\otimes N}$, we calculate the probabilities $P_{\pm\pm\pm\pm}$ that determine the measurement outcomes of the protocol in Sec. I A for the OTOC $\langle \sigma_i^x(t)\sigma_j^x\sigma_i^x(t)\sigma_j^x\rangle$; see Appendix A for detailed expressions for the relevant probabilities. To simulate a finite number of experimental runs of the measurement protocol, we draw pseudorandom numbers according to these probabilities and calculate a finite-sample estimator of $\mathscr{C}$. In Fig. 2 (top), the real part ReC of the exact OTOC is compared to the finite-sample estimator of $2\mathscr{C} - 1$ for samples of size $N_s = 10^4$. While the agreement with the exact result is excellent, small statistical errors are visible in the estimator. To assess the magnitude of the statistical errors, we compare the estimators obtained with sample sizes $N_s = 10^2$, and 10^3 in Fig. 3. Statistical errors are found to decrease quickly with increasing sample size, and a moderate value of $N_s = 10^3$ is sufficient to obtain relative statistical errors of only a few percent.

C. Measurement protocol for the imaginary part

The imaginary part of an OTOC is known to contain information that is complementary to that of the real part [28], and obtaining both is therefore desirable. The corresponding measurement protocol we present here requires, in addition to backward time evolution, the experimental capability to perform single-qubit rotations at sites i and j. The imaginary part of the OTOC (2) can be obtained by the following sequence of operations (see Fig. 1 for an illustration):

(i') Prepare the initial state $|\psi\rangle$.
(ii') Rotate spin j by an angle θ_1 around the b direction.
(iii') Time-evolve unitarily until time t.
(iv') Rotate spin i by an angle θ_2 around the a direction.
(v') Evolve *backwards* in time for a time t.
(vi') Rotate spin j by an angle θ_3 around the b direction.
(vii') Time-evolve unitarily until time t.
(viii') Projectively measure the observable σ_i^a.

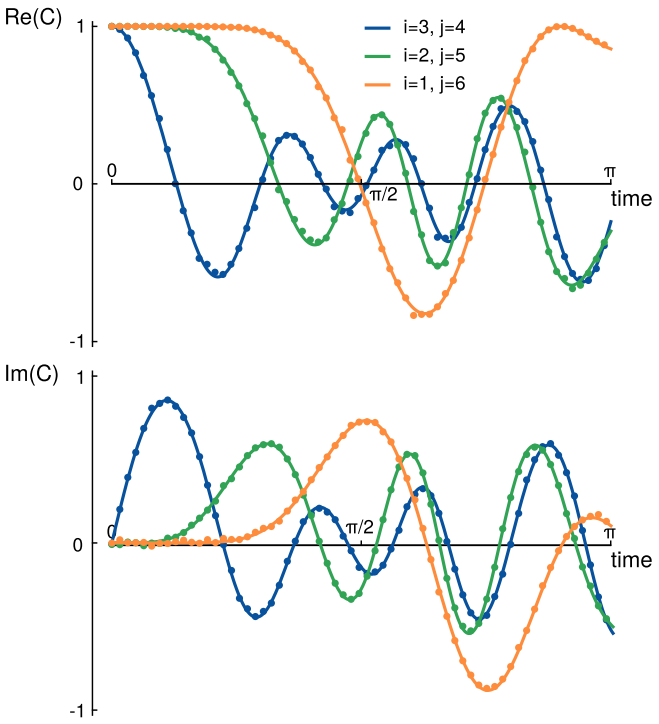

FIG. 2. Real part (top) and imaginary part (bottom) of the OTOC C as a function of time t in an XY spin chain of length N. Different colors correspond to different pairs of lattice sites in definition (2), as specified in the legend. Solid lines show exact results for C, the dots mark estimated values for samples of size 10^4, obtained by calculating the left-hand sides of Eq. (4) for the real part and (6) for the imaginary part, respectively. The further apart the sites i and j, the longer it takes until the OTOC starts to deviate from its initial value, which is a manifestation of quasilocality in a system with short-range interactions.

(ix') Repeat (i')–(viii') many times and record the empirical mean of the measurement outcome.

This empirical mean gives an estimator of the expectation value $\langle \sigma_i^a \rangle_{t,\theta_1,\theta_2,\theta_3}$ with respect to the state at the end of step

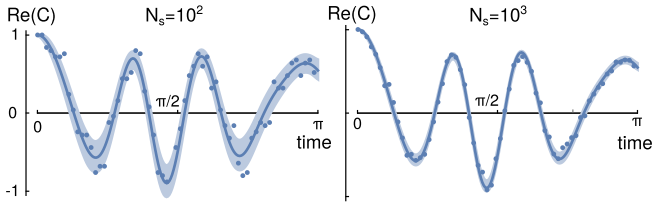

FIG. 3. Magnitude of the statistical fluctuations in the estimator $2\mathscr{C} - 1$, obtained from Eq. (3) and using samples of sizes $N_s = 10^2$ (left) and $N_s = 10^3$ (right). All data are for the OTOC (2) with $i = 2$ and $j = 3$ on a chain of $N = 4$ sites. Solid lines show the exact result, the dots are estimated values, fluctuating around the exact value. The shaded area around the exact result indicates an estimate of the statistical error, obtained by drawing multiple samples, each of size N_s, from the probability distribution of $P_{\pm\pm\pm\pm}$ and then calculate the standard deviation of the estimated values.

(vii') of the above protocol. We show in Appendix B that

$$\begin{aligned}&\langle\sigma_i^a\rangle_{t,-\theta_1,-\theta_2,-\theta_3} - \langle\sigma_i^a\rangle_{t,\theta_1,\theta_2,\theta_3}\\&\quad - \langle\sigma_i^a\rangle_{t,-\theta_1,\theta_2,-\theta_3} + \langle\sigma_i^a\rangle_{t,\theta_1,-\theta_2,\theta_3}\\&\quad = 4\sin(\theta_2)\sin(\theta_1+\theta_3/2)\sin(\theta_3/2)\mathrm{Im}C(t). \qquad (6)\end{aligned}$$

Hence, the imaginary part of the OTOC (2) is obtained by performing the above protocol (i')–(viii') for the four sets of rotation angles $(-\theta_1, -\theta_2, -\theta_3)$, $(\theta_1, \theta_2, \theta_3)$, $(-\theta_1, \theta_2, -\theta_3)$, and $(\theta_1, -\theta_2, \theta_3)$. A simple and, in some sense, optimal choice is $\theta_1 = \theta_2 = \theta_3 = \pi/2$, in which case the right-hand side of Eq. (6) simplifies to $2\mathrm{Im}C(t)$.

A comparison of finite-sample estimators of the left-hand side of Eq. (6) and the exact OTOC is shown in Fig. 2 (bottom). As expected, statistical fluctuations due to finite sample size N_s diminish with increasing N_s, qualitatively similar to the behavior of the real part in Fig. 3 (not shown).

II. EXPERIMENTAL IMPLEMENTATION WITH RYDBERG ATOM ARRAYS

The requirements to implement the above described protocols are coherent forward and backward time evolution under an effective spin-1/2 Hamiltonian, as well as the capability to conduct single-site projective measurements and single-site spin rotations. Among the experimental platforms that allow for coherent dynamics of many-body qubit systems, arrays of ultracold Rydberg atoms in optical tweezers are particularly suitable (see Ref. [29] for a review). Optical tweezers allow the experimenter to arrange and hold the atoms in a lattice geometry of choice, with lattice constants of the order of micrometers. To make the atoms interact over such distances, they are excited to Rydberg states, i.e., atomic states with a large principal quantum number. Various schemes to emulate spin-1/2 Hamiltonians in such arrays have been devised, giving rise to coherent spin dynamics under Ising- or XY-type Hamiltonians. Moreover, single-site control is well established for these platforms [30,31]. In the following we present a solution to the remaining challenge for a successful implementation of our OTOC measurement protocol in Rydberg platforms, namely backwards time evolution or, equivalently, sign inversion of the Hamiltonian.

The experimental scheme we propose is based on microwave-assisted Rydberg dressing [24]. Rydberg dressing naturally leads to spin-1/2 degrees of freedom being encoded in two low-lying and long-lived atomic states, with long-range Ising interactions between the spins [32]. The strength of these interactions can be dynamically tuned by choosing the detuning of the light field, which off-resonantly couples one of the states to a Rydberg state. Several experiments demonstrated this technique in optical lattices and tweezers [33]. The sign of the induced Ising interaction is determined by the sign of the interaction in the laser-addressed Rydberg state. Implementing time reversal with this technique is not straightforward, as it requires the existence of Rydberg states with opposite sign and near-equal magnitude of the interaction potential. Even if a specific pair of Rydberg states is identified that meets this special condition, interaction reversal is still a technically demanding task requiring two distinct laser frequencies.

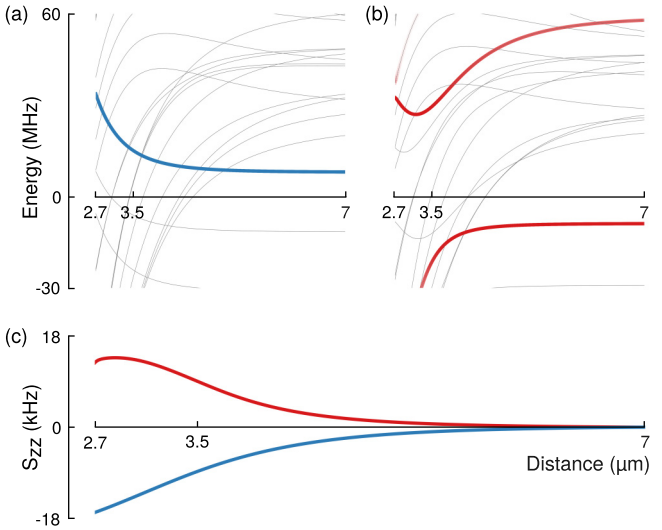

FIG. 4. Illustration of microwave-assisted potential inversion for the example of ^{39}K. (a) Interaction potential between pairs of atoms for various eigenstates of the dipolar interaction. The thick blue line highlights the pair potential between atoms in the $|50S_{1/2}, m_F = 1/2\rangle$ state. The energy corresponding to the laser frequency is chosen as the energy-zero level and the polarization is such that only the highlighted level is coupled from the ground state. (b) Switching on microwave radiation with a frequency of 27.592 GHz, the $|50S_{1/2}, m_J = 1/2\rangle$ state is coupled to the $|50P_{1/2}, m_J = 1/2\rangle$ state. As a result, the pair potentials highlighted as the thick red lines emerge from the blue line in (a) as microwave-dressed pair-states. The plotted data assumes linear polarization and a realistic choice of the Rabi frequency of about 30 MHz. The shading of the colored lines in (a) and (b) is chosen proportional to the laser coupling strength. The weakly visible gray lines indicate other pair states which are not coupled by the laser. (c) Resulting dressed Ising interactions in the electronic ground state for a laser red-detuned by 4 MHz with respect to the single-atom resonance and 4.4 MHz blue-detuned to the lower of the microwave-shifted states. The laser Rabi frequency has been set to 2 MHz. The lower branch arises when the microwave is off from dressing to the highlighted potential in (a), the lower from dressing to the microwave-engineered potentials in (b).

Here we show, for the example of ^{39}K atoms, that this difficulty can be overcome, and sign inversion of the Ising interactions can be implemented, by strong microwave coupling of the van der Waals pair-potential curve to a dipolar potential curve. The blue line in Fig. 4(a) shows the interaction potential between pairs of atoms in the $|50S_{1/2}, m_F = 1/2\rangle$ state, where the zero-energy level is chosen to coincide with the laser with the laser-targeted energy. When switching on microwave radiation with a frequency of 27.592 GHz, the $|50S_{1/2}, m_J = 1/2\rangle$ state is coupled to the $|50P_{1/2}, m_J = 1/2\rangle$ state, resulting in the pair potential shown in red in Fig. 4(b). The splitting of the two emerging potential branches at large distances is determined by the Autler-Townes splitting of the single-atom state. At shorter distances of around 3–4 μm, the signature of an avoided level crossing is visible. For microwave interaction of a suitably chosen strength, the avoided level crossing is opened up to an extent such that the lower branch in Fig. 4(b) becomes the reflection image of the blue line in Fig. 4(a) around the laser-targeted energy. This

property of one pair potential being the reflection image of another then gets imprinted onto the corresponding Ising interactions, as illustrated in Fig. 4(c). These results were obtained with the "pairinteraction" software [34], which diagonalizes the two-atom Hamiltonian, including magnetic fields and dipolar interactions. We extended the software to also include the effect of microwave coupling in the diagonalization. Figure 4(c) illustrates that, by merely switching on or off the microwave-induced coupling, the sign of the Ising interaction is inverted, and hence backward time evolution can be realized. The Rydberg dressing approach discussed here has the advantageous feature that the atoms remain trapped in the optical tweezers during the entire sequence, and that forces between the atoms remain small. This avoids decoherence due to uncontrolled coupling to motional degrees of freedom, which otherwise would corrupt time reversal.

III. SUMMARY AND OUTLOOK

The results presented in this article lay out a path towards measuring OTOCs for arbitrary many-body qubit systems and initial states. Unlike other measurement protocols of that generality, our proposal requires neither randomized measurements nor the use of ancilla degrees of freedom. In our protocol, real and imaginary parts of the OTOC are measured separately, both requiring local control (single-site measurements and single-site rotations, respectively) in the experiment. In addition, coherent forward- as well as backward-in-time evolution are needed.

We demonstrate the feasibility of the proposed measurement protocol for Rydberg-dressed atoms in optical tweezers. While single-site measurements and rotations are readily available in this platform, Hamiltonian sign inversion, which facilitates backward-in-time evolution, has hitherto been missing. We introduced a method that facilitates sign inversion through microwave-assisted Rydberg dressing, thus completing the tool set for successfully implementing our OTOC measurement protocol in arrays of Rydberg atoms. This paves the way for experimental explorations of equilibrium and nonequilibrium situations through OTOCs in these platforms, including the detection of quantum chaos [35], the monitoring of thermalization and the scrambling of quantum information [7,8,28], or more exotic tasks like the probing of excited-state quantum phase transitions [36]. We expect our protocol to become applicable in other many-body qubit systems or analog quantum simulators of spin-1/2 Hamiltonians in the near future.

Note added. Recently, we became aware of Ref. [37], in which sign inversion in a bulk Rydberg gas implementing the dipolar XXZ model was demonstrated.

ACKNOWLEDGMENTS

M.K. gratefully acknowledges useful discussions with A. del Campo and Z.-Y. Xu in an early stage of this project. The authors acknowledge funding from the Deutsche Forschungsgemeinschaft via projects GR 4741/4-1, SPP 1929 GiRyd (GR 4741/5-1) and FOR 5413 (GR 4741/6-1), a Heisenberg professorship (GR 4741/3-1 and GR 4741/7-1) and from the Alfried Krupp von Bohlen und Halbach foundation. This publication has also received funding under the Horizon Europe program HORIZON-CL4-2022-QUANTUM-02-SGA via the project 101113690 (PASQuanS2.1).

APPENDIX A: PROOF OF EQ. (4)

Denote by $\Pi_i^{\pm_a}$ the projector onto the $\pm$ eigenstate of the Pauli operator σ_i^a.

In the course of the protocol (i)–(viii) the system state goes through the following stages:

(i) Initial state ρ.

(ii) After the first measurement, and depending on the outcome $\pm$ of the measurement, the state is

$$\rho_1^{\pm} = \Pi_j^{\pm_b} \rho \Pi_j^{\pm_b} / P_{\pm}, \tag{A1}$$

where

$$P_{\pm} = \mathrm{Tr}\big(\rho \Pi_j^{\pm_b}\big) \tag{A2}$$

is the probability of measuring $+$ or $-$.

(iv) After the second measurement, and depending on the outcome $\pm$ of the first measurement (ii) and the outcome $\pm$ of the second measurement (iv), the state is

$$\rho_2^{\pm\pm} = \Pi_i^{\pm_a} e^{-iHt} \rho_1^{\pm} e^{iHt} \Pi_i^{\pm_a} / P_{\pm|\pm}, \tag{A3}$$

where

$$P_{\pm|\pm} = \mathrm{Tr}\big(e^{-iHt} \rho_1^{\pm} e^{iHt} \Pi_i^{\pm_a}\big) \tag{A4}$$

is the conditional probability of measuring $\pm$ in the second measurement after having measured $\pm$ in the first measurement.

(vi) Similarly one obtains

$$\rho_3^{\pm\pm\pm} = \Pi_j^{\pm_b} e^{iHt} \rho_2^{\pm\pm} e^{-iHt} \Pi_j^{\pm_b} / P_{\pm|\pm\pm} \tag{A5}$$

with

$$P_{\pm|\pm\pm} = \mathrm{Tr}\big(e^{iHt} \rho_2^{\pm\pm} e^{-iHt} \Pi_j^{\pm_b}\big) \tag{A6}$$

after the third measurement.

(viii) And

$$\rho_4^{\pm\pm\pm\pm} = \Pi_i^{\pm_a} e^{-iHt} \rho_3^{\pm\pm\pm} e^{iHt} \Pi_i^{\pm_a} / P_{\pm|\pm\pm\pm} \tag{A7}$$

with

$$P_{\pm|\pm\pm\pm} = \mathrm{Tr}\big(e^{-iHt} \rho_3^{\pm\pm\pm} e^{iHt} \Pi_i^{\pm_a}\big) \tag{A8}$$

after the fourth measurement.

The probability of finding a specific sequence of the four measurement outcomes $\pm$ is then given by

$$P_{\pm\pm\pm\pm} = P_{\pm} P_{\pm|\pm} P_{\pm|\pm\pm} P_{\pm|\pm\pm\pm}. \tag{A9}$$

Inserting Eqs. (A1)–(A9) into the correlation function (3), the latter can be written as

$$\mathscr{C}(t) = \sum_{o_1,o_2,o_3,o_4 \in \{-,+\}} o_1 o_2 o_3 o_4 \times \mathrm{Tr}\big[\Pi_i^{o_4}(t) \Pi_j^{o_3} \Pi_i^{o_2}(t) \Pi_j^{o_1} \rho \Pi_j^{o_1} \Pi_i^{o_2}(t) \Pi_j^{o_3}\big], \tag{A10}$$

where $\Pi_i^o(t) := e^{iHt} \Pi_i^o e^{-iHt}$. Making use of the spectral representation

$$\sigma_i^a = \Pi_i^{+_a} - \Pi_i^{-_a} = \sum_{o_4 \in \{-,+\}} o_4 \Pi_i^{o_4} \tag{A11}$$

as well as the linearity of the trace, one obtains

$$\mathscr{C}(t) = \sum_{o_1,o_2,o_3\in\{-,+\}} o_1 o_2 o_3 \mathrm{Tr}\big[\sigma_i^a(t)\Pi_j^{o_3}\Pi_i^{o_2}(t)\Pi_j^{o_1}\rho\Pi_j^{o_1}\Pi_i^{o_2}(t)\Pi_j^{o_3}\big]. \tag{A12}$$

Using the completeness relation $\Pi_j^{o_3} = \mathbb{1}_j - \Pi_j^{-o_3}$ on the second occurrence of $\Pi_j^{o_3}$ in Eq. (A12), $\mathscr{C}$ can be rewritten as

$$\begin{aligned}\mathscr{C}(t) = &\sum_{o_1,o_2\in\{-,+\}} o_1 o_2 \mathrm{Tr}\left[\sigma_i^a(t)\left(\sum_{o_3\in\{-,+\}} o_3\Pi_j^{o_3}\right)\Pi_i^{o_2}(t)\Pi_j^{o_1}\rho\Pi_j^{o_1}\Pi_i^{o_2}(t)\right]\\ &- \sum_{o_1,o_2,o_3\in\{-,+\}} o_1 o_2 o_3 \mathrm{Tr}\big[\sigma_i^a(t)\Pi_j^{o_3}\Pi_i^{o_2}(t)\Pi_j^{o_1}\rho\Pi_j^{o_1}\Pi_i^{o_2}(t)\Pi_j^{-o_3}\big].\end{aligned} \tag{A13}$$

The second line of (A13) can be simplified by recognizing that the term in round brackets is the spectral representation of $\sigma_j^b = \Pi_j^{+_b} - \Pi_j^{-_b}$. Writing out the remaining o_3 sum in the bottom two lines of (A13) and using the cyclic invariance of the trace, one obtains

$$\begin{aligned}\mathscr{C}(t) = \sum_{o_1,o_2\in\{-,+\}} o_1 o_2 \big(&\mathrm{Tr}\big[\sigma_i^a(t)\sigma_j^b\Pi_i^{o_2}(t)\Pi_j^{o_1}\rho\Pi_j^{o_1}\Pi_i^{o_2}(t)\big] - \mathrm{Tr}\big[\sigma_i^a(t)\Pi_j^{+_b}\Pi_i^{o_2}(t)\Pi_j^{o_1}\rho\Pi_j^{o_1}\Pi_i^{o_2}(t)\Pi_j^{-_b}\big]\\ &+ \mathrm{Tr}\big[\Pi_j^{-_b}\Pi_i^{o_2}(t)\Pi_j^{o_1}\rho\Pi_j^{o_1}\Pi_i^{o_2}(t)\Pi_j^{+_b}\sigma_i^a(t)\big]\big).\end{aligned} \tag{A14}$$

The operator products in the second and third trace in Eq. (A14) are Hermitian conjugates of each other. Hence, the difference of the traces can be expressed as an imaginary part, yielding

$$\mathscr{C}(t) = 2i\ \mathrm{Im}\ c_3 + \sum_{o_1,o_2\in\{-,+\}} o_1 o_2 \mathrm{Tr}\big[\sigma_i^a(t)\sigma_j^b\Pi_i^{o_2}(t)\Pi_j^{o_1}\rho\Pi_j^{o_1}\Pi_i^{o_2}(t)\big] \tag{A15}$$

with

$$c_3 = \sum_{o_1,o_2\in\{-,+\}} o_1 o_2 \mathrm{Tr}\big[\Pi_j^{-_b}\Pi_i^{o_2}(t)\Pi_j^{o_1}\rho\Pi_j^{o_1}\Pi_i^{o_2}(t)\Pi_j^{+_b}\sigma_i^a(t)\big]. \tag{A16}$$

Next we apply the completeness relation $\Pi_i^{o_2} = \mathbb{1}_j - \Pi_i^{-o_2}$ and the corresponding spectral representation to the first occurrence of $\Pi_i^{o_2}$ in Eq. (A15), which yields

$$\mathscr{C}(t) = 2i\ \mathrm{Im}\ c_3 + \sum_{o_1\in\{-,+\}} o_1 \mathrm{Tr}\big[\sigma_j^b\Pi_j^{o_1}\rho\Pi_j^{o_1}\big] - \sum_{o_1,o_2\in\{-,+\}} o_1 o_2 \mathrm{Tr}\big[\sigma_i^a(t)\sigma_j^b\Pi_i^{-o_2}(t)\Pi_j^{o_1}\rho\Pi_j^{o_1}\Pi_i^{o_2}(t)\big]. \tag{A17}$$

Applying the same completeness relation and spectral representation to the second occurrence of $\Pi_i^{o_2}$ in Eq. (A15), one obtains

$$\mathscr{C}(t) = 2i\ \mathrm{Im}\ c_3 + \sum_{o_1\in\{-,+\}} o_1 \mathrm{Tr}\big[\sigma_i^a(t)\sigma_j^b\sigma_i^a(t)\Pi_j^{o_1}\rho\Pi_j^{o_1}\big] + \sum_{o_1,o_2\in\{-,+\}} o_1 o_2 \mathrm{Tr}\big[\sigma_i^a(t)\sigma_j^b\Pi_i^{-o_2}(t)\Pi_j^{o_1}\rho\Pi_j^{o_1}\Pi_i^{o_2}(t)\big]. \tag{A18}$$

Summing Eqs. (A17) and (A18) gives

$$2\mathscr{C}(t) = 4i\ \mathrm{Im}\ c_3 + \sum_{o_1\in\{-,+\}} o_1 \mathrm{Tr}\big[\sigma_j^b\Pi_j^{o_1}\rho\Pi_j^{o_1}\big] + \sum_{o_1\in\{-,+\}} o_1 \mathrm{Tr}\big[\sigma_i^a(t)\sigma_j^b\sigma_i^a(t)\Pi_j^{o_1}\rho\Pi_j^{o_1}\big]. \tag{A19}$$

Similarly, by applying the completeness relation $\Pi_j^{o_1} = \mathbb{1}_j - \Pi_j^{-o_1}$ and the corresponding spectral representation to the second occurrences of $\Pi_j^{o_1}$ in the first as well as the second trace of Eq. (A19), one arrives at

$$2\mathscr{C}(t) = 2i\ \mathrm{Im}(c_2 + 2c_3) + C(t) + 1 \tag{A20}$$

with

$$c_2 = \sum_{o_1\in\{-,+\}} o_1 \mathrm{Tr}\big[\Pi_j^{-_b}\rho\Pi_j^{+_b}\sigma_i^a(t)\sigma_j^b\sigma_i^a(t)\big]. \tag{A21}$$

The first term on the right-hand side of Eq. (A20) is purely imaginary, whereas $\mathscr{C}$ is real by definition (3). Hence, by taking the real part on both sides of the Eq. (A20) one arrives at Eq. (4).

APPENDIX B: PROOF OF EQ. (6)

Spin rotations at the lattice site i around the a axis by an angle θ are described by the unitary rotation operator

$$R_i^a(\theta) = \exp\big(-i\sigma_i^a\theta/2\big) \equiv \cos(\theta/2) - i\sin(\theta/2)\sigma_i^a. \tag{B1}$$

After step (vii') of the rotation protocol the system is in the state

$$\mathscr{R}(t,\theta_1,\theta_2,\theta_3)\,\rho\,\mathscr{R}(t,\theta_1,\theta_2,\theta_3)^\dagger \tag{B2}$$

with

$$\mathscr{R}(t,\theta_1,\theta_2,\theta_3) := e^{-iHt}R_j^b(\theta_3)e^{iHt}R_i^a(\theta_2)e^{-iHt}R_j^b(\theta_1). \tag{B3}$$

Using this expression to calculate the expectation values of σ_i^a on the left-hand side of Eq. (6) results in a lengthy expression

with numerous combinations of sine and cosine terms. Simplifying these terms, either by hand in a tedious calculation or quickly using Mathematica, establishes the validity of Eq. (6). This calculation makes repeated use of the involution $(\sigma_i^a)^2 = \mathbb{1}$, which is an indication that the measurement protocol is unlike to hold beyond bivariate observables.

[1] Y. Sekino and L. Susskind, Fast scramblers, J. High Energy Phys. 10 (2008) 065; S. H. Shenker and D. Stanford, Black holes and the butterfly effect, *ibid.* 03 (2014) 067.

[2] J. M. Deutsch, Quantum statistical mechanics in a closed system, Phys. Rev. A **43**, 2046 (1991); M. Srednicki, Chaos and quantum thermalization, Phys. Rev. E **50**, 888 (1994); C. Gogolin and J. Eisert, Equilibration, thermalisation, and the emergence of statistical mechanics in closed quantum systems, Rep. Prog. Phys. **79**, 056001 (2016).

[3] J. Maldacena, S. H. Shenker, and D. Stanford, A bound on chaos, J. High Energy Phys. 08 (2016) 106.

[4] For unitary operators V and W satisfying $[W, V] = 0$, a short calculation yields $\mathrm{Re}[F(t)] = 1 - \langle|[W(t), V]|^2\rangle/2$.

[5] A. I. Larkin and Y. N. Ovchinnikov, Quasiclassical method in the theory of superconductivity, J. Exp. Theor. Phys. **28**, 1200 (1969).

[6] P. Hosur, X.-L. Qi, D. A. Roberts, and B. Yoshida, Chaos in quantum channels, J. High Energy Phys. 02 (2016) 004.

[7] R. Fan, P. Zhang, H. Shen, and H. Zhai, Out-of-time-order correlation for many-body localization, Sci. Bull. **62**, 707 (2017).

[8] Y. Huang, Y.-L. Zhang, and X. Chen, Out-of-time-ordered correlators in many-body localized systems, Ann. Phys. (Berlin) **529**, 1600318 (2017); X. Chen, T. Zhou, D. A. Huse, and E. Fradkin, Out-of-time-order correlations in many-body localized and thermal phases, *ibid.* **529**, 1600332 (2017).

[9] S. Braun, J. P. Ronzheimer, M. Schreiber, S. S. Hodgman, T. Rom, I. Bloch, and U. Schneider, Negative absolute temperature for motional degrees of freedom, Science **339**, 52 (2013).

[10] D. Linnemann, H. Strobel, W. Muessel, J. Schulz, R. J. Lewis-Swan, K. V. Kheruntsyan, and M. K. Oberthaler, Quantum-enhanced sensing based on time reversal of nonlinear dynamics, Phys. Rev. Lett. **117**, 013001 (2016).

[11] K. A. Gilmore, M. Affolter, R. J. Lewis-Swan, D. Barberena, E. Jordan, A. M. Rey, and J. J. Bollinger, Quantum-enhanced sensing of displacements and electric fields with two-dimensional trapped-ion crystals, Science **373**, 673 (2021).

[12] S. Colombo, E. Pedrozo-Peñafiel, A. F. Adiyatullin, Z. Li, E. Mendez, C. Shu, and V. Vuletić, Time-reversal-based quantum metrology with many-body entangled states, Nat. Phys. **18**, 925 (2022).

[13] B. Vermersch, A. Elben, L. M. Sieberer, N. Y. Yao, and P. Zoller, Probing scrambling using statistical correlations between randomized measurements, Phys. Rev. X **9**, 021061 (2019); P. D. Blocher, S. Asaad, V. Mourik, M. A. I. Johnson, A. Morello, and K. Mølmer, Measuring out-of-time-ordered correlation functions without reversing time evolution, Phys. Rev. A **106**, 042429 (2022).

[14] J. Li, R. Fan, H. Wang, B. Ye, B. Zeng, H. Zhai, X. Peng, and J. Du, Measuring out-of-time-order correlators on a nuclear magnetic resonance quantum simulator, Phys. Rev. X **7**, 031011 (2017).

[15] K. X. Wei, C. Ramanathan, and P. Cappellaro, Exploring localization in nuclear spin chains, Phys. Rev. Lett. **120**, 070501 (2018).

[16] K. A. Landsman, C. Figgatt, T. Schuster, N. M. Linke, B. Yoshida, N. Y. Yao, and C. Monroe, Verified quantum information scrambling, Nature (London) **567**, 61 (2019).

[17] X. Nie, B.-B. Wei, X. Chen, Z. Zhang, X. Zhao, C. Qiu, Y. Tian, Y. Ji, T. Xin, D. Lu, and J. Li, Experimental observation of equilibrium and dynamical quantum phase transitions via out-of-time-ordered correlators, Phys. Rev. Lett. **124**, 250601 (2020).

[18] B. Chen, X. Hou, F. Zhou, P. Qian, H. Shen, and N. Xu, Detecting the out-of-time-order correlations of dynamical quantum phase transitions in a solid-state quantum simulator, Appl. Phys. Lett. **116**, 194002 (2020).

[19] M. K. Joshi, A. Elben, B. Vermersch, T. Brydges, C. Maier, P. Zoller, R. Blatt, and C. F. Roos, Quantum information scrambling in a trapped-ion quantum simulator with tunable range interactions, Phys. Rev. Lett. **124**, 240505 (2020).

[20] B. Swingle, G. Bentsen, M. Schleier-Smith, and P. Hayden, Measuring the scrambling of quantum information, Phys. Rev. A **94**, 040302(R) (2016); L. García-Álvarez, I. L. Egusquiza, L. Lamata, A. del Campo, J. Sonner, and E. Solano, Digital quantum simulation of minimal AdS/CFT, Phys. Rev. Lett. **119**, 040501 (2017).

[21] B. Sundar, A. Elben, L. K. Joshi, and T. V. Zache, Proposal for measuring out-of-time-ordered correlators at finite temperature with coupled spin chains, New J. Phys. **24**, 023037 (2022).

[22] M. Gärttner, J. G. Bohnet, A. Safavi-Naini, M. L. Wall, J. J. Bollinger, and A. M. Rey, Measuring out-of-time-order correlations and multiple quantum spectra in a trapped-ion quantum magnet, Nat. Phys. **13**, 781 (2017); J. Braumüller, A. H. Karamlou, Y. Yanay, B. Kannan, D. Kim, M. Kjaergaard, A. Melville, B. M. Niedzielski, Y. Sung, A. Vepslinen, R. Winik, J. L. Yoder, T. P. Orlando, S. Gustavsson, C. Tahan, and W. D. Oliver, Probing quantum information propagation with out-of-time-ordered correlators, *ibid.* **18**, 172 (2022).

[23] X. Mi, P. Roushan, C. Quintana, S. Mandr, J. Marshall, C. Neill, F. Arute, K. Arya, J. Atalaya, R. Babbush, J. C. Bardin, R. Barends, J. Basso, A. Bengtsson, S. Boixo, A. Bourassa, M. Broughton, B. B. Buckley, D. A. Buell, B. Burkett *et al.*, Information scrambling in quantum circuits, Science **374**, 1479 (2021).

[24] S. Sevinçli and T. Pohl, Microwave control of Rydberg atom interactions, New J. Phys. **16**, 123036 (2014); D. Petrosyan and K. Mølmer, Binding potentials and interaction gates between microwave-dressed Rydberg atoms, Phys. Rev. Lett. **113**, 123003 (2014); R. M. W. van Bijnen and T. Pohl, Quantum magnetism and topological ordering via Rydberg dressing near Förster resonances, *ibid.* **114**, 243002 (2015).

[25] S. Lu, M. C. Bañuls, and J. I. Cirac, Algorithms for quantum simulation at finite energies, PRX Quantum **2**, 020321 (2021).

[26] E. Davis, G. Bentsen, and M. Schleier-Smith, Approaching the Heisenberg limit without single-particle detection, Phys. Rev. Lett. **116**, 053601 (2016); F. Fröwis, P. Sekatski, and W. Dür, Detecting large quantum fisher information with finite

measurement precision, *ibid.* **116**, 090801 (2016); T. Macrì, A. Smerzi, and L. Pezzè, Loschmidt echo for quantum metrology, Phys. Rev. A **94**, 010102(R) (2016).

[27] This strategy has been employed in a different context in Ref. [38].

[28] M. Sajjan, V. Singh, R. Selvarajan, and S. Kais, Imaginary components of out-of-time-order correlator and information scrambling for navigating the learning landscape of a quantum machine learning model, Phys. Rev. Res. **5**, 013146 (2023).

[29] A. Browaeys and T. Lahaye, Many-body physics with individually controlled Rydberg atoms, Nat. Phys. **16**, 132 (2020).

[30] T. M. Graham, Y. Song, J. Scott, C. Poole, L. Phuttitarn, K. Jooya, P. Eichler, X. Jiang, A. Marra, B. Grinkemeyer, M. Kwon, M. Ebert, J. Cherek, M. T. Lichtman, M. Gillette, J. Gilbert, D. Bowman, T. Ballance, C. Campbell, E. D. Dahl *et al.*, Multi-qubit entanglement and algorithms on a neutral-atom quantum computer, Nature (London) **604**, 457 (2022).

[31] D. Bluvstein, S. J. Evered, A. A. Geim, S. H. Li, H. Zhou, T. Manovitz, S. Ebadi, M. Cain, M. Kalinowski, D. Hangleiter, J. P. B. Ataides, N. Maskara, I. Cong, X. Gao, P. S. Rodriguez, T. Karolyshyn, G. Semeghini, M. J. Gullans, M. Greiner, V. Vuletić *et al.*, Logical quantum processor based on reconfigurable atom arrays, Nature (London) **626**, 58 (2024).

[32] L. I. R. Gil, R. Mukherjee, E. M. Bridge, M. P. A. Jones, and T. Pohl, Spin squeezing in a Rydberg lattice clock, Phys. Rev. Lett. **112**, 103601 (2014).

[33] Y.-Y. Jau, A. M. Hankin, T. Keating, I. H. Deutsch, and G. W. Biedermann, Entangling atomic spins with a Rydberg-dressed spin-flip blockade, Nat. Phys. **12**, 71 (2016); J. Zeiher, R. van Bijnen, P. Schauß, S. Hild, J.-y. Choi, T. Pohl, I. Bloch, and C. Gross, Many-body interferometry of a Rydberg-dressed spin lattice, *ibid.* **12**, 1095 (2016); J. Zeiher, J.-Y. Choi, A. Rubio-Abadal, T. Pohl, R. van Bijnen, I. Bloch, and C. Gross, Coherent many-body spin dynamics in a long-range interacting Ising chain, Phys. Rev. X **7**, 041063 (2017); E. Guardado-Sanchez, B. M. Spar, P. Schauss, R. Belyansky, J. T. Young, P. Bienias, A. V. Gorshkov, T. Iadecola, and W. S. Bakr, Quench dynamics of a Fermi gas with strong nonlocal interactions, *ibid.* **11**, 021036 (2021); S. Hollerith, K. Srakaew, D. Wei, A. Rubio-Abadal, D. Adler, P. Weckesser, A. Kruckenhauser, V. Walther, R. van Bijnen, J. Rui, C. Gross, I. Bloch, and J. Zeiher, Realizing distance-selective interactions in a Rydberg-dressed atom array, Phys. Rev. Lett. **128**, 113602 (2022); L.-M. Steinert, P. Osterholz, R. Eberhard, L. Festa, N. Lorenz, Z. Chen, A. Trautmann, and C. Gross, Spatially tunable spin interactions in neutral atom arrays, *ibid.* **130**, 243001 (2023); W. J. Eckner, N. Darkwah Oppong, A. Cao, A. W. Young, W. R. Milner, J. M. Robinson, J. Ye, and A. M. Kaufman, Realizing spin squeezing with Rydberg interactions in an optical clock, Nature (London) **621**, 734 (2023).

[34] S. Weber, C. Tresp, H. Menke, A. Urvoy, O. Firstenberg, H. P. Büchler, and S. Hofferberth, Calculation of Rydberg interaction potentials, J. Phys. B **50**, 133001 (2017).

[35] I. Garcí-Mata, R. A. Jalabert, and D. A. Wisniacki, Out-of-time-order correlations and quantum chaos, Scholarpedia **18**, 55237 (2023); J. R. Gonzlez Alonso, N. Shammah, S. Ahmed, F. Nori, and J. Dressel, Diagnosing quantum chaos with out-of-time-ordered-correlator quasiprobability in the kicked-top model, arXiv:2201.08175.

[36] Q. Wang and F. Pérez-Bernal, Probing an excited-state quantum phase transition in a quantum many-body system via an out-of-time-order correlator, Phys. Rev. A **100**, 062113 (2019).

[37] S. Geier, A. Braemer, E. Braun, M. Müllenbach, T. Franz, M. Grttner, G. Zürn, and M. Weidemüller, Time-reversal in a dipolar quantum many-body spin system, arXiv:2402.13873.

[38] P. Uhrich, S. Castrignano, H. Uys, and M. Kastner, Noninvasive measurement of dynamic correlation functions, Phys. Rev. A **96**, 022127 (2017).